J. Space Weather Space Clim. 2025, **15**, 45
© J.A. Cahuasquí et al., Published by EDP Sciences 2025
https://doi.org/10.1051/swsc/2025040

JSWSC

Available online at:
www.swsc-journal.org

Topical Issue – Swarm 10-Year Anniversary

TECHNICAL ARTICLE OPEN ACCESS

New Swarm products NeGIX and TEGIX for monitoring horizontal ionospheric gradients

Juan Andrés Cahuasquí[1,*], Mohammed Mainul Hoque[1], Norbert Jakowski[1], Stephan Buchert[2], Dmytro Vasylyev[1], Grzegorz Nykiel[1], Paul David[1], Youssef Tagargouste[1], Martin Kriegel[1], Jens Berdermann[1], and Klaus Nielsen[3]

[1] Institute for Solar-Terrestrial Physics, German Aerospace Center (DLR), Kalkhorstweg 53, 17235 Neustrelitz, Germany
[2] Swedish Institute of Space Physics (IRF), Box 537, 751 21, Uppsala, Sweden
[3] Division of Geomagnetism and Geospace, Technical University of Denmark (DTU), Centrifugevej 356, 2800 Kgs. Lyngby, Denmark

Received 4 April 2025 / Accepted 18 September 2025

Abstract – The detection, monitoring, and characterization of ionospheric perturbations are key areas of space weather research due to their significant impact on man-made technological systems. The European Space Agency's (ESA) Swarm mission has provided high-quality data and services for more than 11 years, enriching our understanding of solar, magnetospheric, thermospheric, ionospheric, and atmospheric processes, as well as their coupling and effects on human activities. As part of the Swarm Data, Innovation, and Science Cluster (DISC) project "Monitoring Ionospheric GRAdients at Swarm (MIGRAS)", we have developed two novel Swarm data products to study the state and dynamics of the ionosphere at Swarm height and medium scales – in the order of 100 km. We introduce and validate the electron density spatial gradient index, NeGIX, and the total electron content (TEC) gradient index, TEGIX. We leverage the near-polar, parallel orbits of Swarm A and C to combine data with a resolution of 0.5° in latitude along the satellite tracks. NeGIX uses electron density measurements from the Langmuir Probe experiment onboard Swarm A and C, while TEGIX uses Precise Orbit Determination (POD) data from the Swarm TEC product. We validate these indices for both quiet and perturbed geomagnetic conditions, and further comparison is made with the Swarm Ionospheric Plasma IRregularities (IPIR) product and the ground-based Gradient Ionosphere indeX (GIX). The zonal component of the NeGIX and TEGIX gradients, and particularly their meridional component, clearly identify ionospheric perturbations in the selected case studies. These indices have a high potential for detecting ionospheric perturbations during storm events and provide valuable information about their dynamical evolution. It is expected that NeGIX and TEGIX may essentially support ionospheric research, practical applications, and low-latency monitoring services.

Keywords: Swarm / Ionospheric gradients / NeGIX / TEGIX

1 Introduction

The detection, monitoring, and characterization of small-scale irregularities, as well as medium- and large-scale ionospheric perturbations, are crucial for space weather monitoring services due to their severe and hazardous impact on the functionality of modern radio systems used for telecommunication, navigation, and remote sensing. Although studying ionospheric perturbations is challenging because of their vastly different temporal and spatial scales, several proxies have demonstrated their validity in quantifying these phenomena.

In the *L*-band, ionospheric irregularities at scales ranging from tens to hundreds of meters, which cause amplitude scintillations, are quantified by the *S*4 index. This index is defined as the normalized ratio of the standard deviation of signal intensity fluctuations to the mean signal intensity (Groves et al., 1997; Anderson, 2003; Kintner et al., 2007; Aol et al., 2020; Wu, 2020). Accompanied phase changes caused by ionospheric irregularities on the order of hundreds of meters up to several kilometers can additionally be quantified by the σ_ϕ index (Van Dierendonck et al., 1993; Beach, 2006; Zhao et al., 2022). Another powerful index for detecting and quantifying ionospheric irregularities across various scales is the Rate Of Total electron content Index (ROTI), which is defined as the standard deviation of the rate of change of total electron content (ROT)

*Corresponding author: andres.cahuasqui@dlr.de

This is an Open Access article distributed under the terms of the Creative Commons Attribution License (https://creativecommons.org/licenses/by/4.0), which permits unrestricted use, distribution, and reproduction in any medium, provided the original work is properly cited.

over a specific time interval, typically 5 min (Pi et al., 1997). Moreover, multiple studies have revealed a close relationship between ROTI and the aforementioned scintillation metrics (Olwendo et al., 2018; Carrano et al., 2019; Li et al., 2020).

To estimate the degree of ionospheric perturbation at medium and large scales – such as during the propagation of ionization fronts or traveling ionospheric disturbances spanning several hundred kilometers (Jakowski et al., 2009; Thaganyana et al., 2022) – Jakowski et al. (2006) proposed and Jakowski et al. (2012) further developed the Disturbance Ionosphere indeX (DIX). DIX is a space weather proxy that relies on ground-based global navigation satellite systems (GNSS) measurements of the total electron content (TEC) to quantify the potential impact of ionospheric perturbation events on radio systems. The index utilizes ionospheric pierce points (IPPs) defined by the intersection of radio links between GNSS satellites and receivers with an assumed single-layer ionospheric height (e.g., 350, 400, or 450 km). By taking pairs of IPPs, the ROT between them is estimated. DIX is calculated as a statistical value (e.g., mean or median) derived from all IPP pairs within a predefined region. A generalized definition of DIX includes both temporal and spatial TEC gradients, which can be treated separately. An advanced version of DIX, known as the Disturbance Ionosphere indeX Spatial Gradient (DIXSG, Wilken et al., 2018), has demonstrated the ability to describe regional and global perturbations using link-related spatial TEC gradients. Furthermore, the Gradient Ionosphere indeX (GIX) introduced by Jakowski & Hoque (2019) provides a method for characterizing the absolute value of horizontal TEC gradients instantaneously. This method achieves a latency equal to the time resolution of the input GNSS data and eliminates the need for statistical analyses of historical data. GIX is particularly recommended for exploring regional ionospheric perturbations with scales ranging from a few tens to several hundred kilometers. Spatial scales below 30 km are not considered to avoid high GIX values resulting from dividing differential TEC by short dipole lengths. Conversely, for scales greater than approximately 300 km, GIX becomes smoother and loses the resolution necessary to support precise GNSS applications and Safety-of-Life operations. Recently, Nykiel et al. (2024) tested the relationship between GIX and other ionospheric indices with GNSS positioning degradation, finding that GIX gradients are strongly associated with relative positioning degradation at low and medium latitudes.

Despite their advantages, the aforementioned ionospheric proxies rely primarily on ground-based techniques, which are restricted to observation sites over landmasses. Space-based measurements, in contrast, enable global coverage, including over oceans, but require new and innovative approaches for data analysis to advance space weather science and mitigate associated risks.

Since their launch in November 2013, ESA's Swarm satellites (Friis-Christensen et al., 2008) – Alpha (A), Bravo (B), and Charlie (C) – have provided unparalleled data products and services, significantly enhancing our understanding of solar, magnetospheric, thermospheric, ionospheric, and atmospheric processes, as well as their coupling and impacts on man-made technological systems. Currently, the Swarm Product Data Handbook[1] offers access to 73 Level 1b and Level 2 products derived from Swarm measurements, along with around 16 additional products obtained from other spacecraft and distributed via the Swarm Data, Innovation, and Science Cluster (DISC). Specifically, for the investigation of ionospheric plasma irregularities and perturbations, the in-situ plasma density measurements obtained by the Electric Field Instrument (EFI) onboard the Swarm satellites have enabled detailed structural analyses. These studies include equatorial plasma irregularities or bubbles (Xiong et al., 2016a, 2018; Luo et al., 2019; Jin et al., 2020), as well as plasma irregularities and pressure variations at mid- and high latitudes (Park et al., 2017; Liu et al., 2022; Lovati et al., 2022). Building on EFI data, two key Swarm Level 2 data products have been developed: the Ionospheric Bubble Index (IBI, Park et al., 2013) and the Ionospheric Plasma IRregularities Index (IPIR, Jin et al., 2022). The IBI detects sub-kilometer bubbles in magnetic field measurements, while the IPIR leverages Langmuir Probe (LP) measurements along satellite tracks to estimate electron density gradients at various scales (20, 50, and 100 km). However, for near-polar orbiting satellites like the Swarm trio, plasma irregularities can only be sampled in the meridional direction. As a result, longitudinal structures, such as the large-scale irregularities in the equatorial magnetic region (Xiong et al., 2016a; Aa et al., 2020), remain unresolved.

In this paper, we define and validate two novel data products developed under the Swarm DISC project "Monitoring Ionospheric GRAdients at Swarm (MIGRAS)". These products integrate the GIX methodology with space-based observations of the topside ionosphere captured by the Swarm satellites. We leverage the near-polar orbits (87.3° inclination) of Swarm satellites A and C, which fly side-by-side at an altitude of approximately 470 km and achieve a maximum separation of about 170 km (as of 2025) at the equator. By combining their temporally and spatially related measurements along the tracks, with a latitudinal resolution of 0.5°, we derive two key gradient index products: the spatial electron density gradient index (NeGIX) and the spatial TEC gradient index (TEGIX). This approach capitalizes on the unique configuration and high-quality data of Swarm satellites A and C, enabling the development of products that significantly enhance our understanding of the two-dimensional structure of medium- and larger-scale ionospheric perturbations in the topside ionosphere.

The structure of this paper is as follows: Section 2 introduces and defines the NeGIX and TEGIX indices. Section 3 presents validation results and comparisons with existing ionospheric proxies. Section 4 discusses the potential applications and relevance of the MIGRAS products. Finally, Section 5 outlines the key conclusions of this work.

2 Definition of MIGRAS products

The two MIGRAS products are based on the fundamental principle of the ground-based index GIX (Jakowski & Hoque, 2019). At a given epoch, GIX considers all IPPs formed at the intersection of a single-layer ionospheric model and GNSS-receiver links to create pairs, or dipoles, of calibrated VTEC measurements (referred to as TEC hereafter for simplicity). For each pair of pierce points PP_i and PP_j a central point CP_{ij} is defined between them. At this location, the

[1] https://swarmhandbook.earth.esa.int.

gradient value ∇TEC_{ij} is estimated, with an azimuthal direction δ measured clockwise from North. The gradient is normalized over the distance Δs_{ij} between the pierce points. The zonal (West to East, $\nabla TECX_{ij}$) and meridional (South to North, $\nabla TECY_{ij}$) components of the gradient vector are then calculated as:

$$\nabla TEC\, X_{ij} = \nabla TEC_{ij} \sin \delta, \tag{1}$$

$$\nabla TEC Y_{ij} = \nabla TEC_{ij} \cos \delta. \tag{2}$$

For a predefined region with N such vectors, statistical metrics can be computed separately for the X and Y components, including:

- GIX_{mean} – the mean value of all vectors,
- GIX_{σ} – the standard deviation, or
- GIX_{95p} – the 95th-percentile, representing the most extreme upper or lower values, which is particularly effective for detecting sharp TEC changes, such as those caused by solar flares (Hernández-Pajares et al., 2012; Berdermann et al., 2018) or energetic particle precipitation (Jayachandran et al., 2012).

The same principle of GIX is applied to define NeGIX and TEGIX, with modifications to account for the unique geometrical distribution of measurements and the dynamic and technical characteristics of the Swarm satellites.

Figure 1 illustrates the spatial configuration where NeGIX and TEGIX are defined, highlighting the near-parallel positions of the Swarm satellites A and C and their relationship to the GNSS satellites. Since NeGIX is derived from Level 1b in-situ LP measurements taken by Swarm units A and C, its altitude of definition corresponds to the flight altitude of the satellites. In contrast, the Swarm Level 2 TEC product used for TEGIX calculations, provides absolute vertical TEC values based on the assumption of a height-independent plasma density ionosphere with a thickness of 400 km above the Swarm satellites. These values are nevertheless referenced to the satellites' positions rather than the ionospheric pierce points. To calculate TEGIX, an additional step is performed to infer the locations of the IPPs, along with their respective VTEC values, at an adopted altitude of 200 km above the Swarm satellites. The details of this procedure are described in Section 2.2.

The Earth globe in Figure 2 illustrates schematically the 0.5° latitudinal spatial resolution – equivalent to approximately 8 seconds of flight – used along the satellite tracks for both MIGRAS data products. Due to the near-polar parallel orbits of Swarm satellites A and C, the longitudinal separation of measurements ranges from a few kilometers at the poles to approximately 170 km at the equator. The left side of Figure 2 depicts the combination of electron density measurements used for defining NeGIX, while the right side outlines the methodology adopted for TEGIX. In both cases, only pairs of measurements with distances (Δs_{ij}) between 30 and 200 km are considered. This range is chosen to examine medium-scale perturbations while avoiding the strong sensitivity to data calibration at smaller distances and ensuring coverage of the largest separations achievable with Swarm A and C.

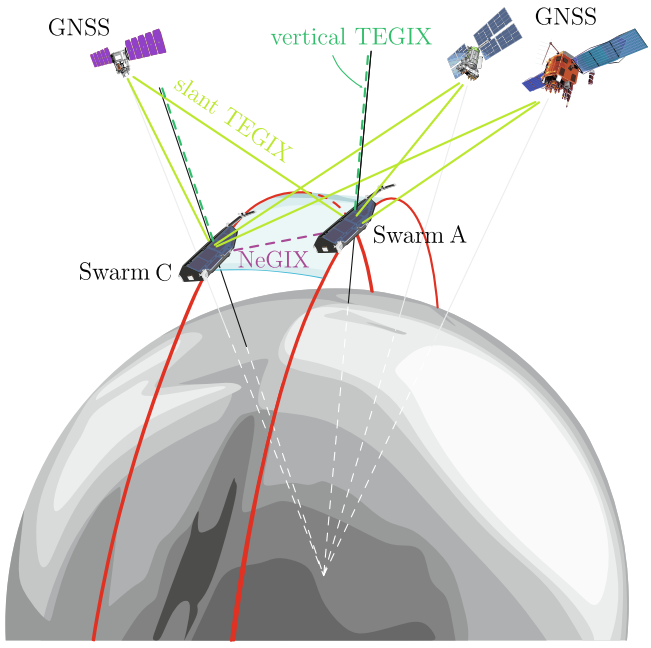

Figure 1. Scheme of the spatial configuration and definition of the MIGRAS products, NeGIX and TEGIX, with respect to the Swarm and GNSS satellites.

2.1 Swarm electron density (Ne) gradient index – NeGIX

NeGIX utilizes electron density measurements acquired in-situ at an altitude of approximately 470 km with the LP instrument onboard the Swarm satellites A and C to monitor medium-scale irregularities with horizontal spatial scales up to 200 km. The Swarm operational (OPER) Level 1b product SW_EFIx_LP_1B,[2] used as input data, is publicly available[3] with a current latency of 4 days. The input daily dataset for each satellite consists of two Extensible Markup Language (XML) files containing metadata and one Common Data Format (CDF) file with plasma density measurements sampled at 2 Hz. This results in approximately 16 data points recorded by each Swarm satellite along a path of 0.5° in latitude.

As shown in the left scheme of Figure 2, gradient vectors are formed between same-satellite measurements (A-A and C-C), as well as zonally between measurements from different satellites. In analogy with the definition of GIX, for instance, for a dipole between t_{A1} and t_{C2} a central point $CP_{t_{C2}-t_{A1}}$ is determined. The gradient vector $\nabla Ne_{t_{C2}-t_{A1}}$ with azimuthal direction δ is estimated, and normalized over the distance $\Delta s_{t_{C2}-t_{A1}}$ between the measurements. Due to the geometry of data combination, the origin of the transversal NeGIX vectors lies on the midpoint trace of the satellites, whereas for the vectors between same-satellite measurements, the origin lies on their respective satellite tracks. Then, the statistical metrics $NeGIX_{mean}$, $NeGIX_{\sigma}$, and $NeGIX_{95p}$ of the resulting NeGIX, and its zonal and meridional components, are calculated from all available vectors over the given resolution sectors.

[2] https://swarmhandbook.earth.esa.int/catalogue/SW_EFIx_LP_1B.
[3] https://swarm-diss.eo.esa.int/#swarm%2FLevel1b%2FEntire_mission_data%2FEFIx_LP.

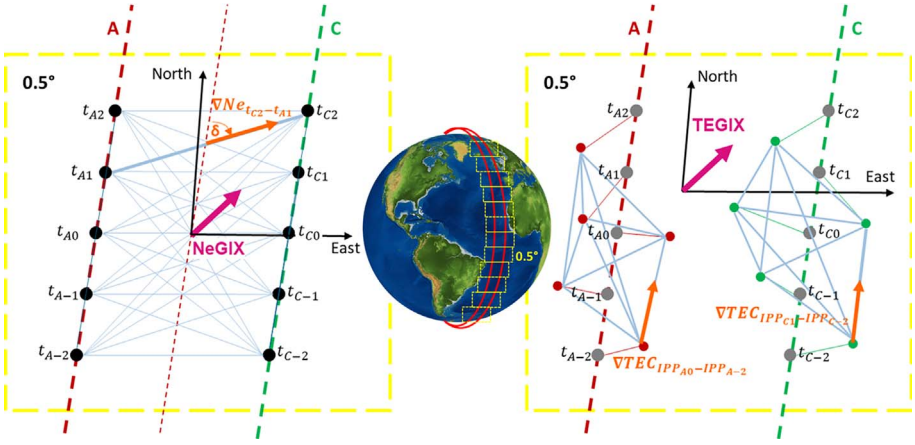

Figure 2. Illustration of the horizontal definition of the MIGRAS products NeGIX (left) and TEGIX (right). Both Swarm data products utilize measurements from Swarm satellites A and C, with a latitudinal resolution of 0.5° along their orbital paths, as shown on the Earth globe in the center. The data combination approach for their definition differs due to the geometry of in-situ LP measurements for NeGIX and the availability of GNSS-derived TEC data for TEGIX.

In accordance with the description of flagged measurements in the Swarm Level 1b Product Definition,[4] only measurements with nominal data (values $\leq$20 in the Flags_Ne parameter) are used for dipole formation. Although Lomidze et al. (2018) proposed a correction factor for Swarm LP measurements of 1.1067 for Swarm A, and 1.1157 for Swarm C, these corrections are not applied to NeGIX calculations due to their negligible effect on gradient estimations.

The resulting time series and metadata of the NeGIX product (SW_NIX_TMS_2F) are stored as daily CDF and metadata files, following the conventions established for ESA's Swarm mission.[5] A detailed description of the product variables contained in the CDF file is provided in Appendix A.

2.2 Swarm TEC Gradient IndeX – TEGIX

TEGIX uses as input the publicly available [6] Swarm OPER Level 2 data product SW_TECxTMS_2F [7] from spacecraft A and C to monitor TEC gradients with horizontal spatial scales of up to 200 km. The current latency of these daily files on the Swarm Data Access portal is 5 days. The input dataset for each satellite consists of two XML files containing metadata and one CDF file with Precise Orbit Determination (POD) and TEC measurements at a 1-second resolution [8]. The POD and TEC data from the input products are used to estimate the location of IPPs and their associated VTEC, assuming a "center of mass" height at 200 km above the Swarm satellites. Several articles have reviewed and used a similar procedure of IPP determination (Klobuchar, 1987; Sharma et al., 2018; Prol et al., 2025). At these IPP locations, the slant TEC values provided in the input file are converted to VTEC using the following expressions (Foelsche & Kirchengast, 2002):

In this equation, H_{mapping} is the ionospheric reference height at 200 km above the Swarm satellites, R_S is the height of the Swarm spacecraft, and the parameter r is defined as:

$$\text{VTEC} = \text{STEC} \cdot M(\epsilon), \tag{3}$$

where the mapping function M, as a function of the elevation angle ϵ, is defined as:

$$M(\epsilon) = \frac{H_{\text{mapping}}}{R_S + H_{\text{mapping}}} \left[\cos(\sin^{-1}(r \cdot \cos\epsilon)) - (r \cdot \sin\epsilon)\right]^{-1}. \tag{4}$$

$$r = \frac{R_S}{R_S + H_{\text{mapping}}}. \tag{5}$$

TEGIX is defined with a latitudinal resolution of 0.5°. Unlike the in-situ measurements, the number of possible pair combinations depends on the simultaneous availability of multiple GNSS satellites connected with Swarm A and C throughout the given resolution. As depicted in the right scheme of Figure 2, gradient vectors are formed only between IPPs related the same-satellite measurements (e.g. $\nabla\text{TEC}_{IPP_{A0}-IPP_{A-2}}$ or $\nabla\text{TEC}_{IPP_{C1}-IPP_{C-2}}$). The purpose is avoiding potential inconsistencies in the differential code bias (DCB) estimation of onboard GNSS receivers, which is conducted daily and separately for Swarm A and C. According to the Swarm L2 TEC Product documentation, the uncertainty of the input TEC product is 2 TECU,[9] where daily DCB errors exceeding this threshold are flagged. Jakowski & Hoque (2019) similarly considered an uncertainty of 1 TECU in the calculation of GIX. However, even if any TEC input file contains daily receiver DCB errors larger than 2 TECU, this is not expected to affect TEGIX gradient estimates as the dipole formations rely exclusively on the same-satellite receiver measurements.

[4] https://earth.esa.int/eogateway/documents/20142/37627/swarm-level-1b-product-definition-specification.pdf.
[5] https://swarmhandbook.earth.esa.int/documents/d/earth-online/swarm-level-2-product-specification.
[6] https://swarm-diss.eo.esa.int/#swarm%2FLevel2daily%2FEntire_mission_data%2FTEC%2FTMS.
[7] https://swarmhandbook.earth.esa.int/catalogue/SW_TECxTMS_2F.
[8] https://earth.esa.int/eogateway/documents/20142/37627/swarm-level-2-tec-product-description.pdf.
[9] 1TECU = 1000 mTECU=10^{16} elm^{-2}

When calibrating Swarm POD TECs, the DCBs of the GNSS satellites are considered as known parameters and taken from the International GNSS Service (IGS). Their accuracies are within fractions of TECU. Therefore, the satellite DCB errors will not essentially impact the TEGIX accuracy.

The resulting TEGIX over the given resolution sector can be deduced from all available vectors jointly for Swarm A and C, and expressed as the statistical proxies $TEGIX_{mean}$, $TEGIX_{\sigma}$, and $TEGIX_{95p}$ – also for their zonal and meridional components. The right illustration of Figure 2 shows that the origin of the resulting TEGIX vector is not necessarily symmetric with respect to satellites A and C but varies depending on the availability of GNSS records. The resulting time series and metadata of the TEGIX product, SW_TIX_TMS_2F, are exported as daily CDF and header files in accordance with ESA's established conventions. A description of the product variables contained in the CDF file is provided in Appendix B.

3 Validation of data products

3.1 MIGRAS products during quiet geomagnetic conditions

In this section, we demonstrate the capability of NeGIX and TEGIX to characterize ionospheric features during periods of nominal geomagnetic activity. We analyze Swarm data collected on May 9, 2024, a day marked by quiet conditions, with a Kp index of approximately 1 and a Disturbance Storm (Dst) index value that rounded 20 nT over the day. On that day, the Swarm satellites A and C, operating at an average altitude of 479 km, observed the most significant geomagnetic activity during their descending orbits, which included an equatorial pass at 19:16 Local Time (LT). In contrast, the ascending orbits of the satellites observed weakened geomagnetic conditions, with an equatorial pass at 07:16 LT. The ascending orbits are excluded from this analysis because they exhibit minimal to no significant gradient activity.

Figure 3 presents a visualization of the final MIGRAS products for the descending orbits on May 9, 2024. From top to bottom, the left panels display: (*a*) a global map of the in-situ electron density measurements from the LP instruments on Swarm A and C, (*b*) the 95th-percentile results of NeGIX for the zonal component, and (*c*) the 95th-percentile results for the meridional component. Similarly, the right panels present: (*d*) a VTEC map generated from the TEC data of Swarm A and C, (*e*) the 95th-percentile results for the zonal component of TEGIX, and (*f*) the 95th-percentile values for the meridional component of TEGIX.

The equatorial ionization anomaly (EIA) crests, observed in both the plasma density and TEC data of Figure 3, are well characterized by the gradient estimations of NeGIX and TEGIX. In particular, NeGIX not only captures the double positive-negative peaks at equatorial latitudes through the meridional component (panel *c*), but it also reveals weaker gradients in the zonal direction (panel *b*). The estimation of the meridional component of the TEC gradient index (panel *f*) accurately reflects the TEC enhancements observed in panel *d*. However, the zonal component (panel *e*) does not show significant variations in TEC. This can be attributed to two main factors. First, at lower latitudes, the absence of a zonal component is explained by the TEGIX definition, which avoids combining TEC measurements from Swarm A and C across-track to prevent DCB biases. Second, at high and polar latitudes, the geometry of the GNSS satellites with respect to the Swarm satellites – specifically the GPS constellation with an inclination of about 55° – limits the availability of information on TEC gradients in the West-East direction.

A more detailed overview of a sample of Swarm orbits from May 9, 2024, is shown in Figure 4. The figure presents three descending passes over the Atlantic Ocean at longitudes 13°W, 36°W, and 60°W, from top to bottom. The approximate equatorial crossing times for these orbits correspond to Universal Times (UTs) at 20:03, 21:37, and 23:11. The 95th-percentile values for TEGIX_X_P95, TEGIX_Y_P95, NeGIX_X_P95, and NeGIX_Y_P95 are plotted as functions of magnetic quasi-dipole latitude. For comparison with the newly developed products, the rightmost panels of the figure also show the electron density gradient at 100 km from the Swarm IPIR product.

Several observations can be made from Figure 4. First, the equatorial crests and the perturbations at polar regions are the strongest ionospheric features in these profiles, with amplitudes reaching up to 50 mTECU km^{-1} for TEGIX_Y_P95, and 2000 cm^{-3} km^{-1} for NeGIX_Y_P95. The meridional metrics reflect a rather symmetrical equatorial zone with respect to the magnetic equator – especially during the first sample – with crests extending well within ±20 degrees in latitude. The zonal component of NeGIX also shows strong gradients in the equatorial regions, though without clear symmetry as a function of latitude. For reasons outlined above, the zonal component of TEGIX remains relatively unchanged along low- and mid-latitudes. We observe fluctuations at high and polar latitudes that demonstrate the complex and patchy structure of these regions.

Both the Swarm IPIR product and the NeGIX product utilize Swarm Level 1b SW_EFIx_LP_1B measurements as input data to estimate electron density gradients. In the case of the IPIR product, the electron density gradients (Grad_Ne_at_100 km, Grad_Ne_at_50 km, and Grad_Ne_at_20 km) are calculated for each Swarm satellite using running windows of 27, 13, and 5 data points, which correspond to spatial scales of 100, 50, and 20 km, respectively (Jin et al., 2022). The gradient values at these three scales are very similar, with the shortest scale noisier and the largest scale of 100 km smoother. Since these gradient estimations are made along the satellite paths, the meridional component of NeGIX is, by definition, equivalent to these proxies and serves as an ideal test for validation. The key difference between the IPIR gradients and NeGIX is that, by combining across-track data from Swarm A and C within a 0.5° latitudinal resolution – generally 16 data points from each satellite – NeGIX includes gradient scales ranging from 30 to 200 km, consists of a more robust statistical sample, and exclusively provides additional information about the zonal variation of electron density. The zonal electron density gradients between Swarm A and C are primarily attributed to their difference in local time under unperturbed ionospheric conditions (Xiong et al., 2016b). Given the current longitudinal separation of approximately 1.4° between the two satellites, this difference corresponds to about 6 min. Additionally, a longitudinal dependence of the electron density gradients between Swarm A and C has been identified and attributed to

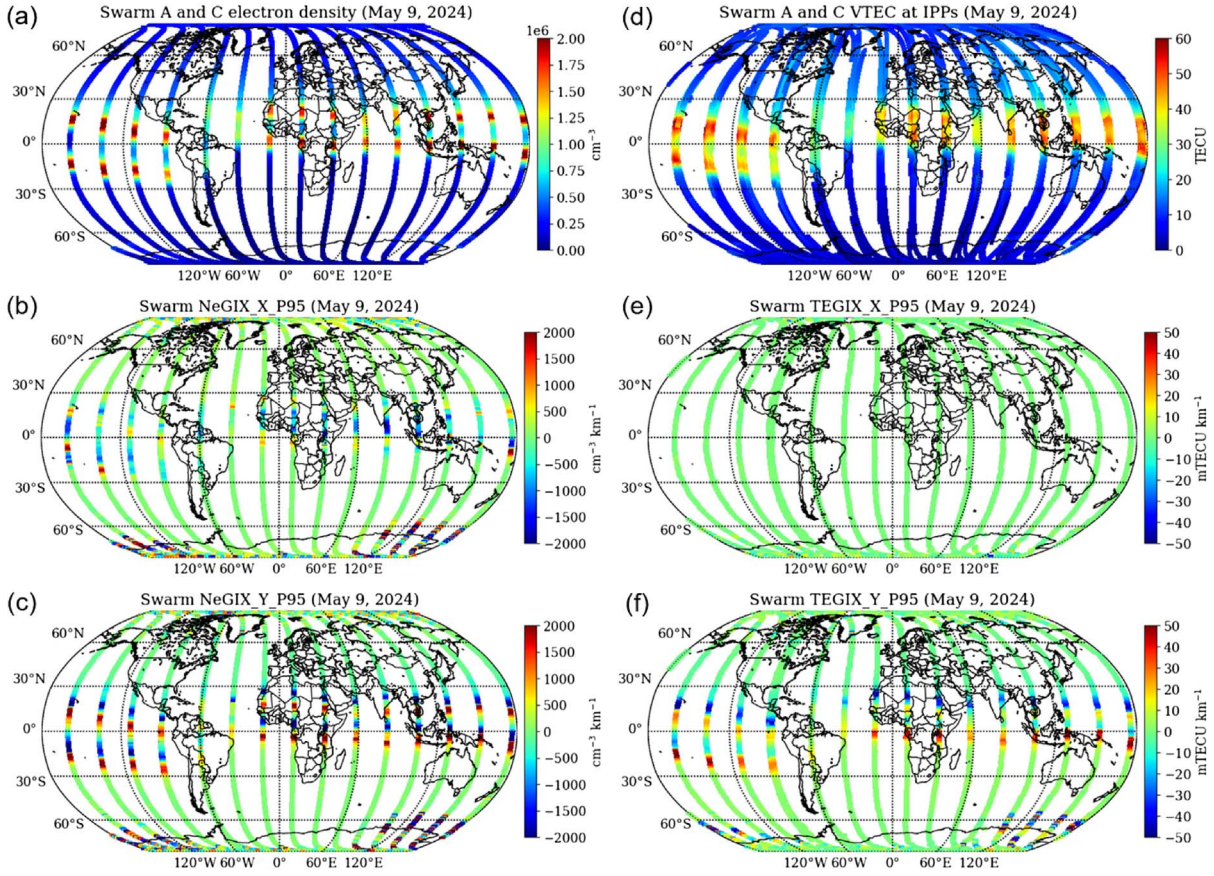

Figure 3. A visualization of the MIGRAS products for the quiet day of May 9, 2024, is shown here. Panel *a* displays an electron density map derived from the EFI Level 1b input data of Swarm A and C, while panel *d* presents a VTEC map created from the Level 2 TEC product of the satellites. The Swarm spacecraft, in their descending orbits shown here, passed over the *equator at 19:16 LT*. The 95th-percentile metrics for NeGIX (panels *b* and *c*) and TEGIX (panels *e* and *f*) are shown for both their zonal and meridional components.

tidal forcing from the lower atmosphere (Xiong et al., 2016b; Zhou et al., 2016). Furthermore, zonal gradients can arise when satellites A and C traverse distinct plasma density structures in the ionosphere. For instance, equatorial plasma irregularities may exhibit plasma density scale sizes smaller than 44 km in the zonal direction (Xiong et al., 2016a), implying that strong gradients can be expected within the scale ranges considered for the NeGIX definition.

Also, the great correlation between NeGIX_Y_P95 and Grad_Ne_at_100 km in Figure 4 led us to conclude that the 95th-percentile values of the gradients are a better statistical proxy for characterizing the ionosphere. Although not plotted in the panels with the purpose of better visualization, the derived mean values of the gradients (variables NeGIX_X and NeGIX_Y in Appendix A) underestimate the real magnitude of variability in the ionosphere due to the unsteady geometry of vectors considered for the computation. Preference for the 95th-percentile metric has also been noted by Jakowski & Hoque (2019) due to its potential to represent better extreme and abrupt changes in the state of the ionosphere.

An analysis of a larger dataset from the NeGIX product is presented in the distribution density plot in Figure 5. The analysis focuses on the period of minimal geomagnetic activity in 2019, which marks the end of Solar Cycle 24. Figure 5 shows the northern summer months (May to July) and the diurnal local time range from 9:00 to 15:00. The data was recorded by Swarm A and C during their descending orbits. The NeGIX_X_P95 (left panel) and NeGIX_Y_P95 (right panel) are plotted as functions of magnetic quasi-dipole latitude, with the color scale indicating the occurrence (counts) of the gradient values over the whole period. Both the zonal and meridional gradients lie within a range of ±500 cm^{-3} km^{-1}. This narrow distribution of values is further depicted by the corresponding histograms displayed in the bottom panels.

The mid-latitudinal zones between approximately ±30° and ±60° show the smallest gradients, while a broader distribution of values is observed at the equatorial crests (peaking around ±15°) and at high latitudes (above ±75°). As seen also in the individual passes of Figure 4, the long-term dataset in Figure 5 clearly delineates the double positive-negative gradient pattern of NeGIX_Y_P95 at the equatorial crests. The right panel also reveals a rather symmetrical distribution of gradient values in the northern polar region and gradients that predominantly favor negative values in the southern polar region. The zonal NeGIX_X_P95 shows a rather uniform distribution of gradient values in the West and East direction at equatorial latitudes. At high latitudes, the gradient values are highly variable, indicating irregular structures caused, probably, by particle precipitation.

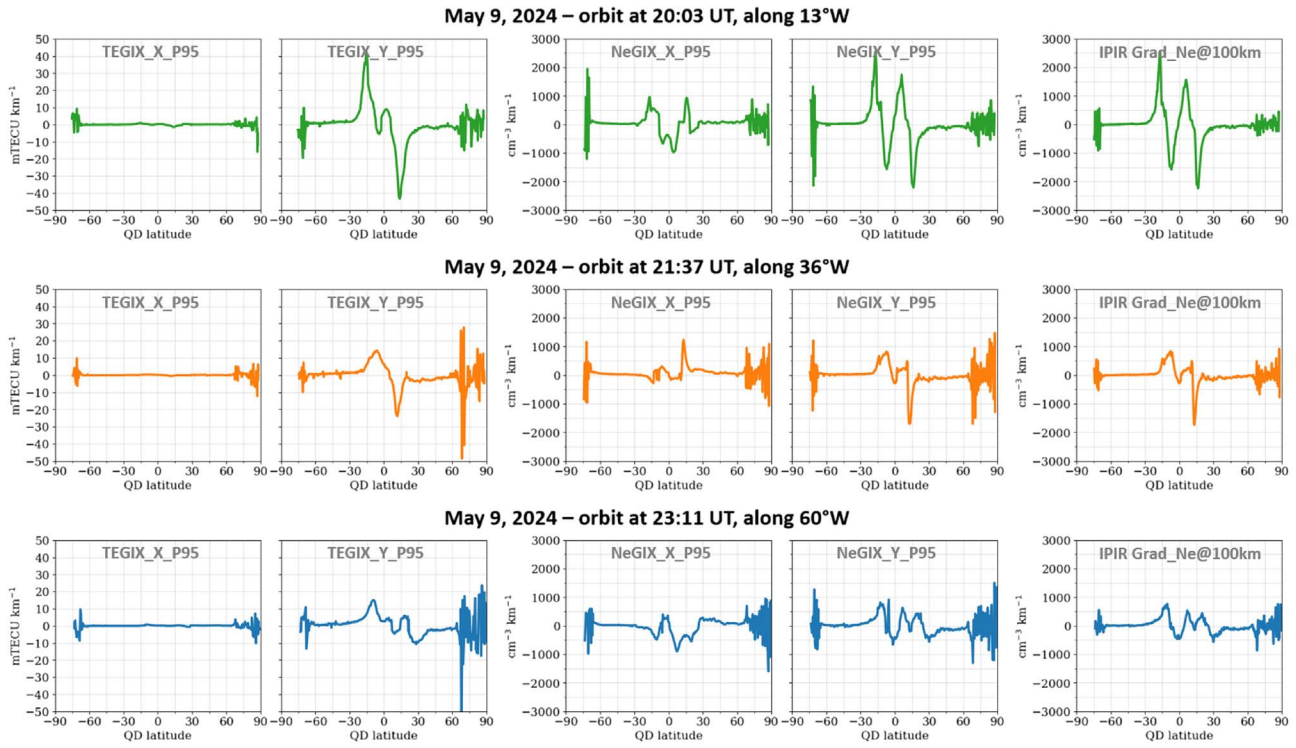

Figure 4. A sample of the TEGIX and NeGIX products for May 9, 2024, as a function of magnetic quasi-dipole latitude, is shown. From top to bottom, the 95th-percentile values of the zonal and meridional components of the gradients are presented in different colors for three Swarm descending orbits, along longitudes over the Atlantic Ocean at 13°W, 36°W, and 60°W. For comparison with an existing Swarm data product, the rightmost panels display the electron density gradients at 100 km, as estimated by the IPIR index.

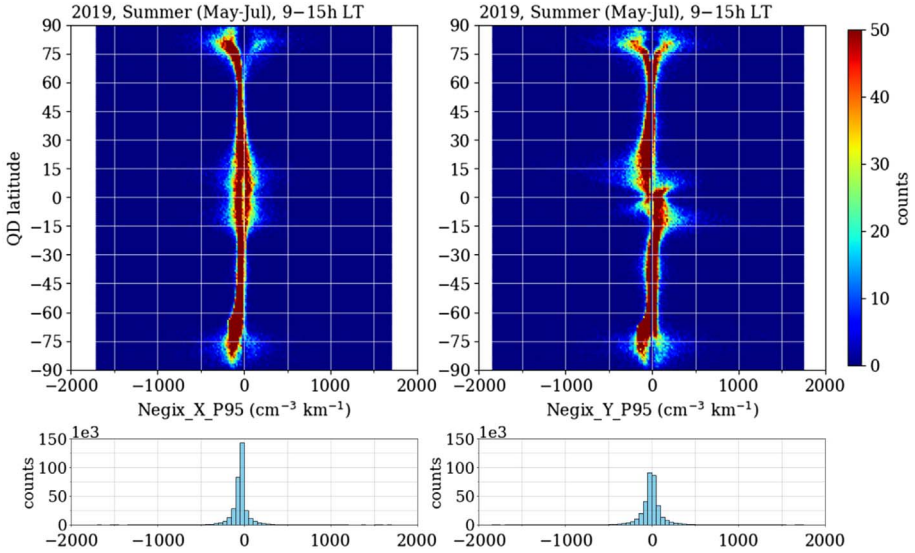

Figure 5. Distribution density plot of NeGIX gradients showing a sample of Swarm A–C data collected during their descending orbits. The period corresponds to the northern summer months (May to July) of 2019, during diurnal local time from 9:00 to 15:00. The 95th-percentile magnitudes of NeGIX_X_P95 (left panel) and NeGIX_Y_P95 (right panel) are plotted as functions of quasi-dipole latitude, with the color scale representing the occurrence (counts) of values. The bottom panels display histograms projecting the distribution of gradient values for both NeGIX components.

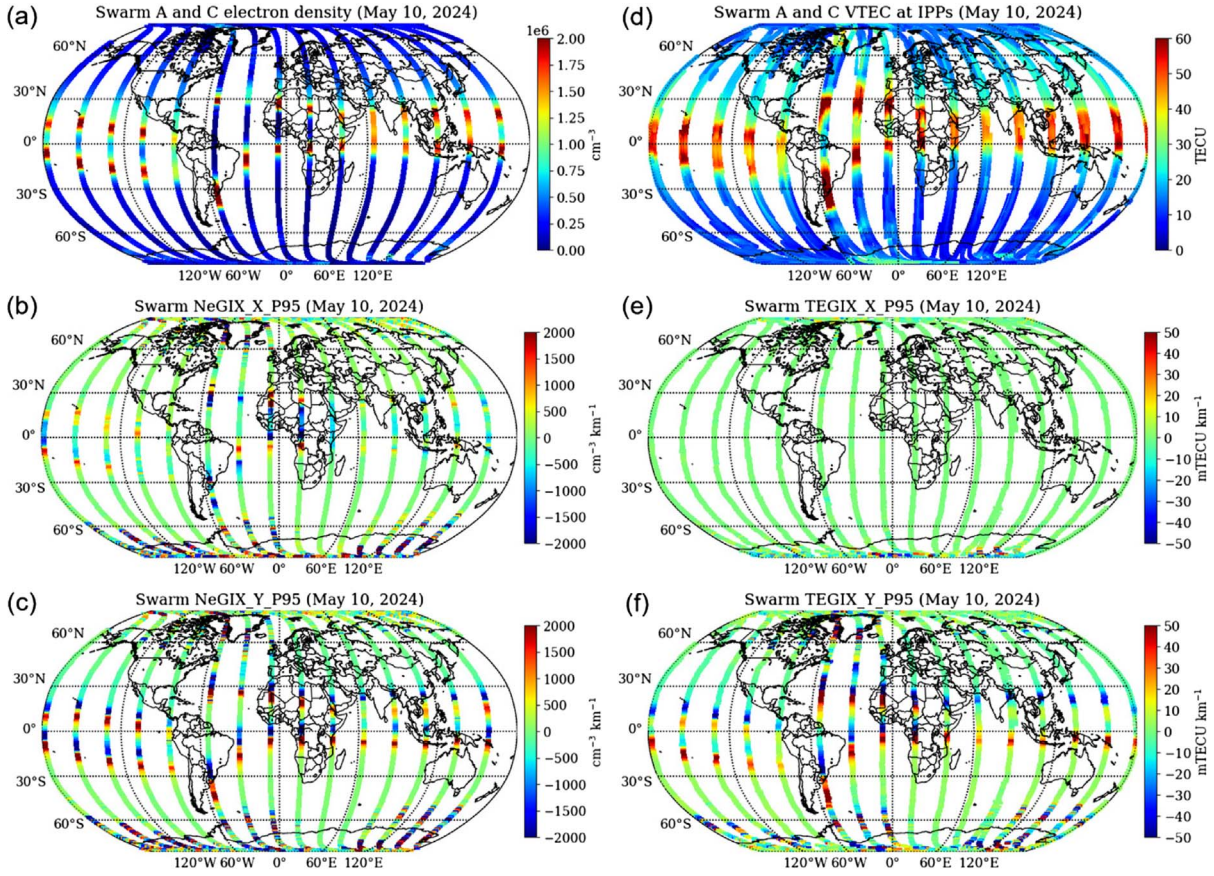

Figure 6. Visualization of the MIGRAS products for the Mother's Day geomagnetic storm on May 10, 2024. Panel *a* shows an electron density map derived from the EFI Level 1b input data of Swarm A and C, while panel *d* displays a VTEC map created from the Level 2 TEC product of the satellites. The Swarm spacecraft, during their descending orbits, had an *equatorial pass at around 19:11 LT*. The 95th-percentile metrics of NeGIX (panels *b* and *c*) and TEGIX (panels *e* and *f*) are shown for their zonal and meridional components.

3.2 MIGRAS products during severely disturbed geomagnetic conditions

The G5-level geomagnetic storm on May 10, 2024, also known as the Mother's Day storm, is presented as a case study due to its status as one of the strongest events of Solar Cycle 25. The main phase of the storm began with a sudden commencement at around 17:00 UT on May 10, reached its peak intensity (Dst index of −412 nT) at approximately 02:00–02:15 UT on May 11, and then entered a recovery phase that extended over the following one to two days (Kwak et al., 2024). The Swarm A and C satellites recorded the most intense geomagnetic activity during their descending node, with an equatorial crossing at around 19:11 LT. Global maps of these passes on May 10 are presented in Figure 6. Given the time of storm onset, the overpasses recorded over Asia occurred beforehand and remained unaffected, whereas those over Western Europe and the Americas sampled the main phase.

In analogy with Figure 3, Figure 6 presents a visualization of the final MIGRAS products for the descending orbits on May 10, 2024. From top to bottom, the left panels display: (*a*) the in-situ electron density measurements plotted over a global map, (*b*) the 95th-percentile results of NeGIX for the zonal component, and (*c*) the 95th-percentile results for the meridional component. Similarly, the right panels present: (*d*) a VTEC map generated from measurements with Swarm A and C, (*e*) the 95th-percentile results for the zonal component of TEGIX, and (*f*) the 95th-percentile values for the meridional component of TEGIX.

In comparison to the conditions presented above for May 9, the Swarm electron density and TEC data acquired on May 10 exhibit much stronger and extended EIA crests and high-latitude perturbations. Particularly, the meridional components of NeGIX and TEGIX shown in panels *c* and *f* reflect strong gradients in low latitudes extending into mid-latitude regions. The northern and southern polar regions also show significant perturbations that spread towards lower latitudes. Indeed, on this day, observers from various mid- and low-latitude locations worldwide witnessed auroral events caused by this intense geomagnetic storm (Gonzalez-Esparza et al., 2024; Grandin et al., 2024; Kataoka et al., 2024). Impacts on space weather, observed through both ground- and space-based instruments, have also been documented (Aa et al., 2024; Spogli et al., 2024). Although with less pronounced signatures, NeGIX_X_P95 shown in panel *b* of Figure 6 also displays electron density gradients in the zonal direction.

Figure 7 presents an overview of three passes over the Atlantic sector, specifically along the longitudes 7°W, 30°W,

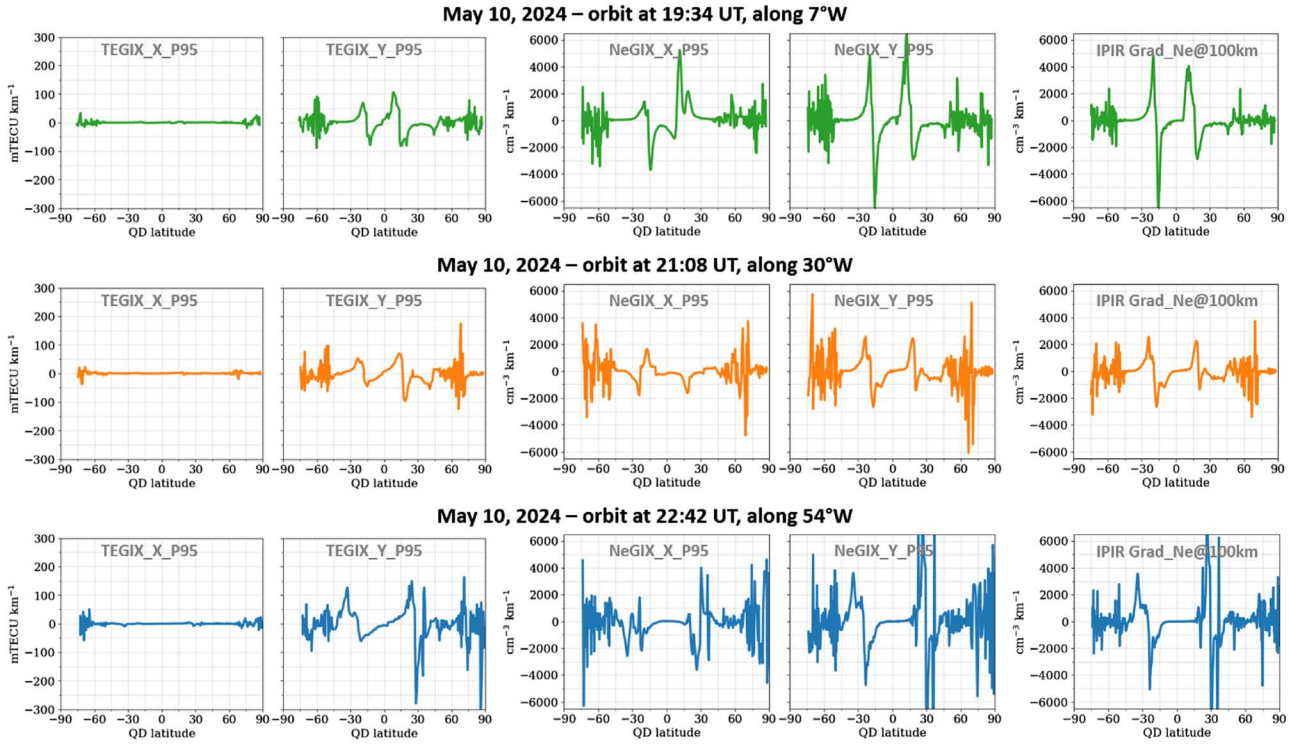

Figure 7. A sample of the TEGIX and NeGIX products for the storm on May 10, 2024, as a function of magnetic quasi-dipole latitude, is shown. The 95th-percentile values of the zonal and meridional components of the gradients are presented in different colors for three Swarm descending orbits, from top to bottom, along longitudes over the Atlantic Ocean at about 7°W, 30°W, and 54°W. The rightmost panels show the electron density gradients at 100 km from the Swarm IPIR product.

and 54°W, from top to bottom. The Swarm orbits correspond to equatorial passes at 19:34, 21:08, and 22:42 UT. In a manner similar to Figure 4, from left to right, the magnitudes of the 95th-percentile values of TEGIX_X_P95, TEGIX_Y_P95, NeGIX_X_P95, and NeGIX_Y_P95 are plotted as functions of magnetic quasi-dipole latitude. For comparison, the Swarm product Grad_Ne_At_100 km is also shown in the rightmost panels.

A notable observation from the Swarm maps in Figure 6 and their related latitudinal profiles in Figure 7 is the extended and asymmetric distribution of the EIA crests over the South American and Atlantic sectors. While plasma accumulation generally occurs near ±15° in geomagnetic latitude (Appleton, 1946, 1954), the crests in this region extend beyond ±30°. This has been noted also by Nayak et al. (2025). The latitudinal profiles of TEGIX and NeGIX in Figure 7 clearly feature the crests' asymmetry with respect to the magnetic equator. The solar wind and interplanetary magnetic field during the exceptional super storm of May 10 clearly led to the unusual location of the EIA crests, but questions and a more quantitative analysis remain (Fejer et al., 2024).

The amplitude values of the profiles in Figure 7 surpass 100 mTECU km^{-1} for the meridional component of TEGIX (as seen for the orbits at 21:08 and 22:42 UT), and above 6000 cm^{-3} km^{-1} for the meridional components of NeGIX and IPIR. The observed TEGIX and NeGIX values are approximately 2 and 3 times greater, respectively, than those observed during the quiet day. Except for the flat profiles of TEGIX_X_P95 due to reasons noted earlier, the other indices display strong, perturbed, and variable features across low-, mid-, and high-latitudes. The double-peak EIA crests observed in latitudinal traces are broad and asymmetric with respect to the magnetic equator, often merging with the strong perturbations observed at latitudes above ±60° (for example, in the Swarm orbit along 54°W shown in blue). Moreover, in this case study, the comparison of our NeGIX_Y_P95 index with Grad_Ne_At_100 km, which yields identical results, serves again to validate its definition and effectiveness in characterizing ionospheric perturbations at medium-range scales.

As in the case reviewed for 2019, the results of a larger dataset for the NeGIX gradients are presented in Figure 8. The dataset corresponds to the diurnal local time from 9:00 to 15:00 during the northern summer months (May to July) of 2024 – a period of strong geomagnetic activity as Solar Cycle 25 approaches its peak in 2025. The data were collected by Swarm A and C during their descending orbits.

The zonal 95th-percentile component (left panel) and the meridional 95th-percentile component (right panel) are plotted as functions of magnetic quasi-dipole latitude, with the color scale representing the occurrence of values. Both the color plots and the histograms in the bottom panels reveal a much broader distribution of gradient values in comparison to the period of quiet conditions. The gradients easily reach ±1000 cm^{-3} km^{-1} at the peaks of the equatorial crests (around ±15°) and at latitudes above ±75°. Extreme cases within this period, such as the Mother's Day storm discussed earlier, exceed largely the ranges shown in Figure 8.

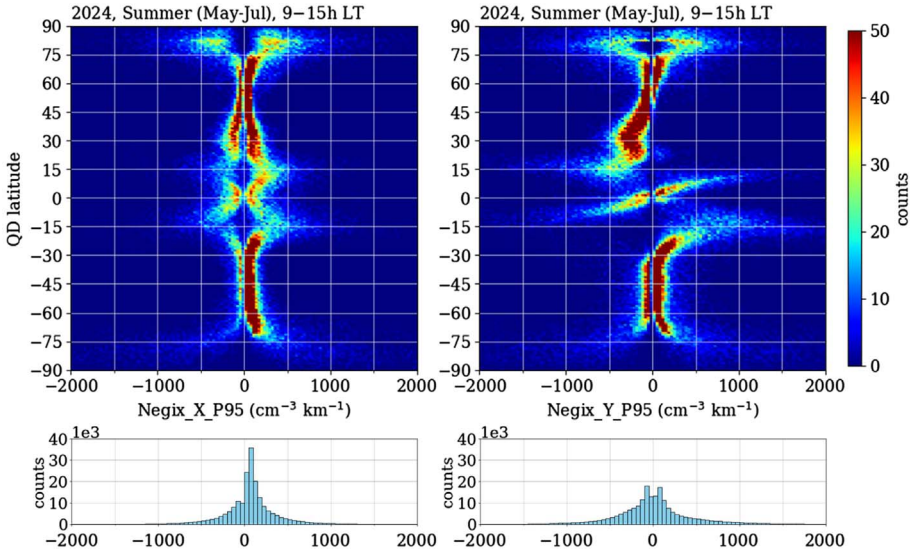

Figure 8. Distribution density plot of NeGIX gradients showing a sample of Swarm A–C data collected during their descending orbits. The period corresponds to the northern summer months (May to July) of 2024, during diurnal local time from 9:00 to 15:00. The magnitudes of NeGIX_X_P95 (left panel) and NeGIX_Y_P95 (right panel) are plotted as functions of quasi-dipole latitude, with the color scale representing the occurrence (counts) of values. The lower panels display histograms showing the distribution of gradient values for both NeGIX components.

The broadly distributed double-peak structure of the EIA is clearly visible in the visualization of NeGIX_Y_P95. Additionally, a clear feature of the ionospheric equatorial trough is observed, indicative of periods of stronger ionization during the daytime and higher solar activity. The longitudinal dependence of the gradients is not visible from this illustration. It is also important to note the differences between the northern and southern high-latitudes (above ±75°). In the northern hemisphere, the gradients seen in NeGIX_X_P95 and NeGIX_Y_P95 remain more confined within a ±1000 cm^{-3} km^{-1} range, while the gradients in the southern hemisphere broadly extend across the entire range. The density plot of the zonal component on the left panel further reveals strong values in the EIA and trough regions, predominantly exhibiting eastward values across all latitudes.

3.3 MIGRAS products compared with the GIX index

Here, we present a comparison of NeGIX and TEGIX with the corresponding ground-based index GIX. As a case study we review the St. Patrick's Day storm on March 17, 2015. This storm was one of the most severe geomagnetic events of Solar Cycle 24 and its impact on space weather has been investigated in numerous studies (Astafyeva et al., 2015; Nava et al., 2016; Maurya et al., 2018). In particular, this event has also been used to validate the ability of GIX to characterize the perturbation degree of the ionosphere at medium scales over Europe and to compare it with other proxies of geomagnetic activity, such as Dst, the Sudden Ionospheric Disturbance indeX (SIDX), and ROTI (Jakowski & Hoque, 2019; Nykiel et al., 2024).

Figure 9 presents a comparison among NeGIX, TEGIX, and GIX, from top to bottom. Two ascending orbits of Swarm A and C over Europe, with equatorial passes at 19:48 LT, are illustrated. On that day, the spacecraft observed minimal geomagnetic activity during their descending paths, and therefore, no sample is presented here. The left-side plots show the estimated mean values of the eastward and northward components of the gradients for the passage over Europe at around 19:00 UT. Similarly, the right-side plots depict the observations for the Swarm passage recorded around 20:30 UT.

For the maps depicted in Figure 9, GIX was computed for a scale comparable to the Swarm products, considering a range from 30 to 200 km. For this purpose, 30-second GNSS data from approximately 350 stations belonging to the EUREF Permanent GNSS Network (EPN) was VTEC calibrated with the methodology proposed by Ma & Maruyama (2003). Also, gradient vectors as described in Section 2 were formed assuming an IPP height of 350 km and considering, for a given epoch, links between the same satellite and all available ground stations within the given range. The studies cited previously have demonstrated the capability of GIX to monitor large-scale ionization fronts propagating in the southwest direction. Such a front can also be noted from the panels for the GIX northward gradients of the figure. NeGIX and TEGIX clearly capture these perturbations, aligning well with the magnitudes and locations of the ground-based index. The strong agreement among these indices is particularly evident for the northward components, as demonstrated also in the latitudinal profiles of Figure 10. A sharp decline in gradient values is observed along the ionization front between 40°N and 55°N, while strong and variable perturbations are seen at latitudes above 55°. Although with a lower degree of correlation, the eastward components of the gradients also reveal signatures of the perturbed ionosphere during these passes. Specifically, the zonal gradients of NeGIX (blue traces) show a significant decline in the electron density gradients of around 250 cm^{-3} km^{-1}, extending between 30°N and 55 N, and strong, variable perturbations up to 300 cm^{-3} km^{-1} above 55°N. The eastward GIX (green traces) closely follows the

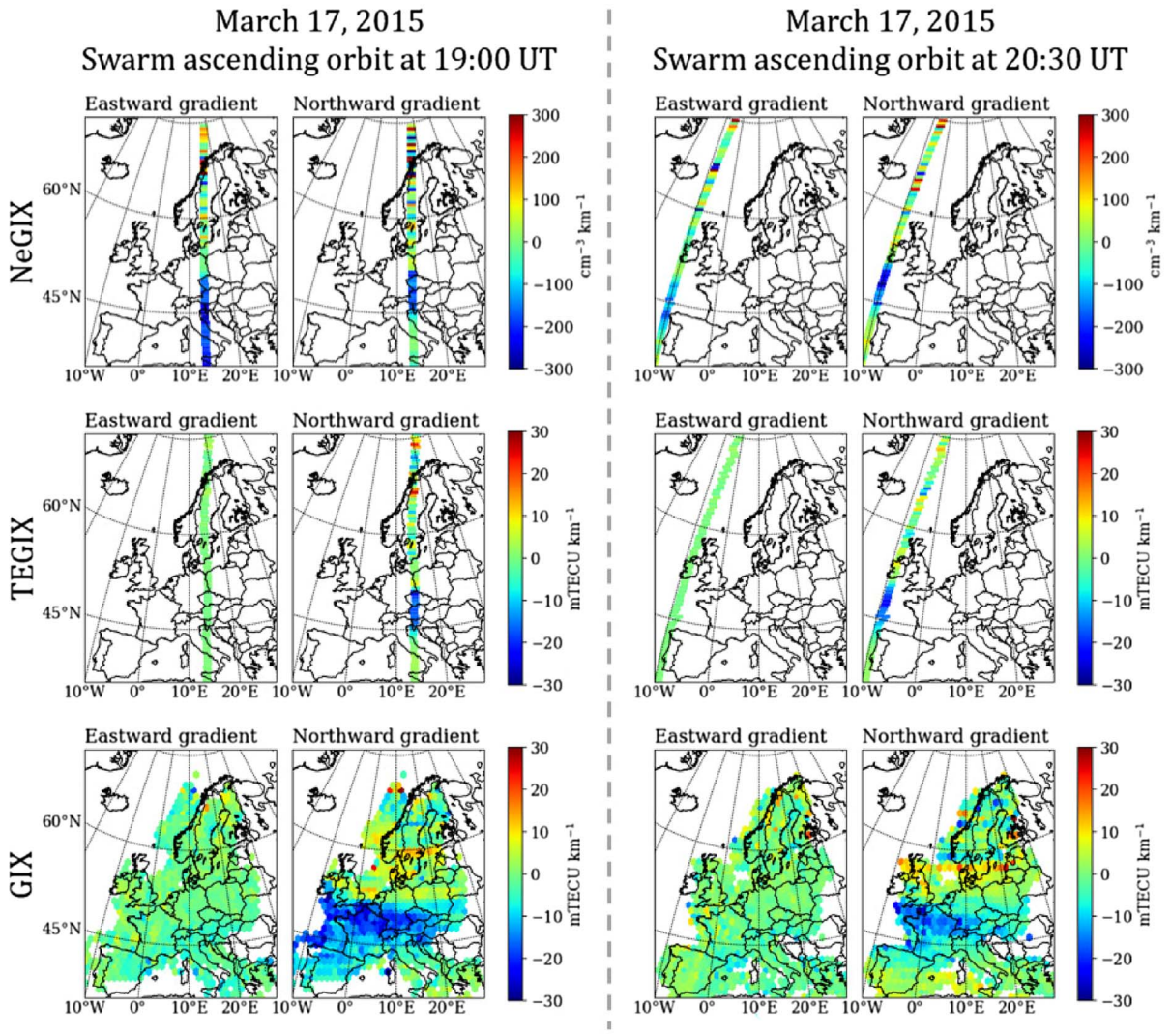

Figure 9. A comparison of the zonal and meridional components of NeGIX, TEGIX, and GIX is presented for two ascending orbits of Swarm A and C on March 17, 2015. The Swarm spacecraft, on this day, passed over the *equator at 19:48 LT*. The left panels show the observations for the pass over Europe around 19:00 UT, while the right panels display the results for the pass around 20:30 UT. Complementarily, Figure 10 shows the profiles of the indices values as a function of latitude for the two orbits.

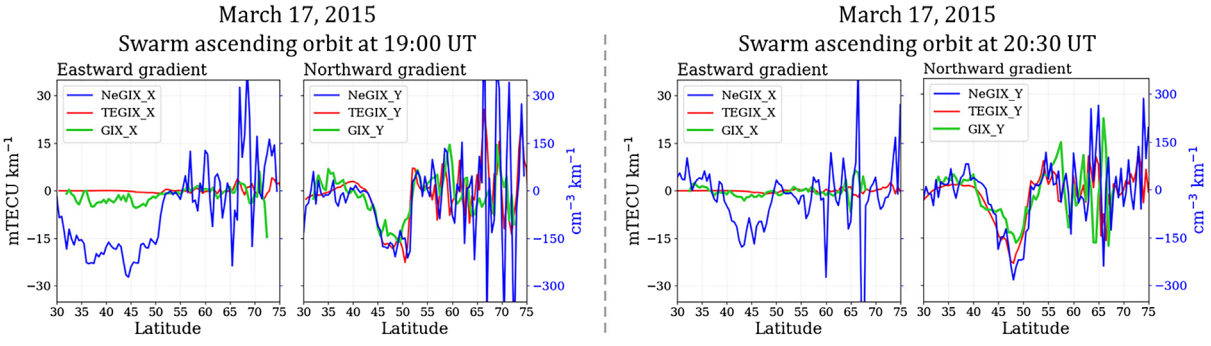

Figure 10. Comparison among the mean values of gradient components of NeGIX (blue), TEGIX (red), and GIX (green) as a function of latitude. The observations correspond to the St. Patrick's Day storm of 2015 as mapped in Figure 9. The two ascending orbits of Swarm A and C above Europe are displayed: the pass around 19:00 UT (left panels) and the pass around 20:30 UT (right panels).

shape of the NeGIX estimation, although with a much smaller amplitude. The eastward component of TEGIX (red traces) remains relatively flat, with only small variations in the TEC index observed above 65°N. Due to the inclusion of the plasmasphere content in TEC data that is clearly dominating in TEGIX, zonal gradients should be principally smooth. Somewhat enhanced dynamic is expected during sunrise and sunset conditions.

It is important to note that the difference in the profiles shown in Figure 10 may arise also from the measurement configurations used to estimate the gradients, or from differences in how the three data products are defined. Electron density gradients are a local characteristic of the ionosphere state with respect to altitude, whereas VTEC gradients are an integral characteristic, meaning some variability may be smoothed out. NeGIX is defined at the altitude of the Swarm satellites A and C (463 km on March 17, 2015), while the IPP points deduced for estimating TEGIX were located at a height of 663 km. On the other hand, as previously mentioned, a single-layer ionosphere at 350 km was assumed to calculate GIX.

4 Discussion

In the previous section, we defined and tested the capabilities of the NeGIX and TEGIX indices to characterize medium-scale ionospheric perturbations. These perturbations were examined during individual geomagnetic events as well as over long seasonal datasets, including both quiet conditions and periods of increased geomagnetic activity. We validated the newly developed Swarm data products using existing products such as the Swarm IPIR index and the ground-based GIX index based on GNSS measurements.

We observe a strong correlation when comparing NeGIX and TEGIX to the existing Swarm IPIR product, especially for the meridional components. A key difference from the IPIR gradients is that NeGIX and TEGIX use data from both Swarm A and C within a 0.5° latitudinal resolution, making the sample used to estimate ionospheric gradients more robust and the results statistically significant. Additionally, both NeGIX and TEGIX provide gradient information along not only the meridional component but also the zonal direction – a feature not available in the existing Swarm data products.

The comparison of the results from NeGIX and TEGIX with GIX also shows strong agreement, particularly in their meridional components. Differences between their profiles may stem from variations in their technical definitions and the geometry of the measurements used to compute the gradients. Since these indices are defined at different altitudes, they can be used complementarily to investigate altitude-related dependencies in horizontal electron density gradient structures. By comparing gradient estimates across the three distinct altitude ranges, we can gain a deeper understanding of the dynamics of ionospheric storms and assess the applicability of the Swarm products. NeGIX and TEGIX can be combined also with other proxies of geomagnetic activity such as the $S4$ index, SIDX, and ROTI to expand our understanding of the processes driving space weather events. By contrasting these indices, we can determine how strongly they correlate one another and whether one index can substitute another. Initial efforts to develop a combined observational study of scintillation events in southern Europe – incorporating NeGIX, TEGIX, and GIX – have already been reported (Morozova et al., 2025).

The algorithms developed to compute the NeGIX and TEGIX indices require only a few minutes of processing time, making them, in principle, well suited for near-real-time monitoring of ionospheric conditions. In practice, however, several factors limit their operational applicability.

First, because NeGIX and TEGIX rely on the orbital geometry of Swarm A and C, a single nearly longitude-aligned strip is sampled only twice per day (ascending and descending nodes). Achieving global coverage with only ascending or only descending passes requires an entire day, and the Swarm satellites cover all local times only about every four months. As a consequence, short-lived or rapidly evolving regional features can be undersampled in space and time.

The dependence on quasi-simultaneous data availability from Swarm A and C presents another limitation. Any missing data from one or both satellites, due to technical issues or calibration problems, can affect the estimation of gradient indices. During the lifetime of Swarm A and C, there have been periods of maneuvering[10] when their separation fell below the minimum required range of 30 km for calculating NeGIX and TEGIX, potentially leading to data quality degradation or missing data[11]. Such issues also arise during time intervals when the Swarm satellites A and C, in their regular near-parallel orbits, reduce their separation to only a few kilometers while crossing over the poles.

A further caveat is data latency. Swarm OPER products typically become available with a delay of at least four days, which can be reduced to about 12 hours (two updates per day) using the advantages of the Fast Track (FAST) method (Orr et al., 2024). Nevertheless, even this enhanced latency is insufficient for near-real-time monitoring and forecasting of ionospheric conditions, which are critical for space-weather services, natural-hazard warnings, and augmentation systems. Ultimately, as is inherent to all mission-dependent products, the continuity of NeGIX and TEGIX is constrained by the stability and lifetime of Swarm A and C.

Within these constraints, the newly developed space-based gradient indices can provide valuable support for the post-event characterization of ionospheric perturbations, particularly for GNSS operators and users in regions with limited ground-based coverage, such as oceans or sparsely populated areas. NeGIX and TEGIX can serve as valuable tools for studying the impact of space weather on precision and Safety-of-Life applications, as well as on augmentation systems like the European Geostationary Navigation Overlay Service (EGNOS). These systems, which rely on trans-ionospheric signals, are particularly vulnerable to ionospheric perturbations. Such perturbations can lead to significant disruptions along satellite-receiver links due to severe spatial gradients and rapid fluctuations in electron density and TEC.

Additionally, these gradients are useful for investigating the mechanisms behind ionospheric storms. Horizontal gradients,

[10] https://earth.esa.int/eogateway/missions/swarm/constellation-and-orbit-evolution.

[11] https://earth.esa.int/eogateway/news/swarm-alpha-and-charlie-orbit-raise-campaign-starting-on-26-april-2023-potential-impact-on-data-quality.

from a mathematical perspective, clearly represent spatial structures, making them well-suited to study dynamic ionospheric processes such as those observed during geomagnetic storms. The temporal variation and the different behaviors of the eastward and northward gradient components can help us to understand the storm propagation mechanisms. Moreover, the distinction between the zonal and meridional components of these indices can provide new insights into the impact of the solar terminator on ionospheric variability and, consequently, on the propagation and deflection of radio waves (Cameron et al., 2024).

The capability of NeGIX and TEGIX to characterize horizontal gradients is of great interest for studying ionospheric processes at both high and low latitudes. At high latitudes, strong gradients at the borders of ionization patches are often linked to enhanced scintillation activity in GNSS signals, due to gradient instability effects in the ionospheric plasma (De Franceschi et al., 2008). At low latitudes, sharp gradients are associated with plasma bubbles, which can also lead to increased scintillation occurrences in GNSS measurements. Due to the disentanglement into zonal and meridional components of these ionospheric indices, it is possible to relate the gradients with the scintillation occurrence and morphology of ionospheric variability (Cesaroni et al., 2015). Indeed, scintillation modeling is another important area that can benefit from NeGIX and TEGIX. For instance, Vasylyev et al. (2024) used electron density gradients from NeGIX to simulate scintillation events in both low- and high-latitude regions, contributing to the development of a phase gradient screen approach.

NeGIX and TEGIX time series – spanning more than 11 years – hold substantial potential for developing and validating empirical and numerical ionospheric models. Combining these indices with measurements from other satellite missions and ground-based observations will further enhance both their scientific value and their practical applications. Finally, the data-combination method developed for Swarm can also be considered for future satellite missions with similar objectives.

5 Conclusions

In the context of the MIGRAS project, we have used the near-parallel orbits of Swarm A and C to develop two innovative data products. These products are unique in their approach of combining Swarm measurements, enabling the estimation of horizontal spatial gradients in electron density and TEC within the topside ionosphere at scales ranging from 30 to 200 km.

We have introduced a detailed technical definition of NeGIX and TEGIX, and demonstrated their capability to monitor and characterize ionospheric perturbations. Testing was conducted for periods of quiet geomagnetic activity – such as the quiet day of May 9, 2024, and the summer diurnal period of 2019 – as well as for perturbed conditions, including the Mother's Day storm on May 10, 2024, and the summer diurnal period of 2024.

Further validation was achieved through comparisons with the Swarm IPIR product and the ground-based GIX index. The results highlight the strong correlation and potential of these indices to monitor the state and dynamics of the ionosphere at medium scales. A key advantage of the NeGIX gradient, compared to the existing IPIR gradients, is its use of across-track data from Swarm satellites A and C at a 0.5° latitudinal resolution. This approach provides a more robust sample for estimating gradients, yielding statistically significant results. Additionally, NeGIX and TEGIX offer gradient information not only along the meridional track of the satellites, as with existing Swarm data products, but also in the West-East direction. This expands our capability to explore the longitudinal morphology of ionospheric perturbations.

The comparison of NeGIX and TEGIX with GIX also opens the possibility of investigating altitude-related dependencies in horizontal gradient structures. Unlike GIX or other ground-based proxies, these new Swarm indices can support research and post-processing applications in regions with limited data availability, such as over oceans or sparsely populated areas. Their practical use, nevertheless, is subject to several constraints. The functionality, data availability, and latency of both Swarm spacecraft A and C are critical factors. A separation of less than 30 km between the satellites, technical maneuvers, or calibration issues affecting either spacecraft can lead to data quality degradation or gaps. At present, the availability of the OPER products used as inputs are subject to a latency of at least four days, although this can be reduced to about 12 h through the FAST data dissemination method. Such latency, however, still precludes the use of these indices for near-real-time monitoring.

We have also discussed the wide range of scientific and practical applications for these indices, including their utility in space weather research, precision and Safety-of-Life applications, augmentation systems, scintillation modeling, and combined observational studies. Additionally, NeGIX and TEGIX can contribute to the development of new empirical and numerical models, as well as low-latency services. The daily OPER products, NeGIX (SW_NIX_TMS_2F) and TEGIX (SW_TIX_TMS_2F), are now publicly available through the official Swarm Data Access at https://swarm-diss.eo.esa.int and the Ionospheric Monitoring and Prediction Center (IMPC) of DLR at https://impc.dlr.de.

In conclusion, NeGIX and TEGIX represent valuable tools for advancing our understanding of ionospheric dynamics and their impact on technology and space weather. The continued development and dissemination of these indices may provide crucial support for both scientific research and practical applications in the monitoring and prediction of ionospheric conditions.

Acknowledgments

The authors gratefully appreciate the technical input provided by Lars Tøffner-Clausen from DTU during the development of the MIGRAS data products. We also thank ESA for operating the Swarm satellite mission and for making the data available to the community. Our gratitude extends to the anonymous referees and the editor for their valuable feedback. The editor thanks two anonymous reviewers for their assistance in evaluating this paper.

Funding

This work is partially funded by ESA via the MIGRAS project under the Swarm DISC Subcontract SW-CO-DTU-GS-133.

Data availability statement

All data used and generated in this study are publicly available through the Swarm Data Access at https://swarm-diss.eo.esa.int.

References

Aa, E, Zhang S-R, Lei J, Huang F, Erickson PJ, Coster AJ, Luo B. 2024. Significant midlatitude plasma density peaks and dual-hemisphere SED during the 10–11 May 2024 super geomagnetic storm. *J Geophys Res Space Phys* **129**: e2024JA033360. https://doi.org/10.1029/2024JA033360.

Aa, E, Zou S, Eastes R, Karan DK, Zhang S-R, Erickson PJ, Coster AJ. 2020. Coordinated ground-based and space-based observations of equatorial plasma bubbles. *J Geophys Res Space Phys*, **125**: e2019JA027569. https://doi.org/10.1029/2019JA027569.

Anderson, DN. 2003. Forecasting the occurrence of ionospheric scintillation activity in the equatorial ionosphere on a day-to-day basis. *GPS Solu* **7**: 200–202. https://doi.org/10.1007/s10291-003-0064-4.

Aol, S, Buchert S, Jurua E. 2020. Ionospheric irregularities and scintillations: a direct comparison of in situ density observations with ground-based L-band receivers. *Earth Planets Space* **72**: 164. https://doi.org/10.1186/s40623-020-01294-z.

Appleton, EV. 1946. Two anomalies in the ionosphere. *Nature*, **157 (3995)**: 691. https://doi.org/10.1038/157691a0.

Appleton, EV. 1954. The anomalous equatorial belt in the F2-layer. *J Atmos Sol-Terr Phys* **5** (**1–6**): 348–351. https://doi.org/10.1016/0021-9169(54)90054-9.

Astafyeva, E, Zakharenkova I, Förster M. 2015. Ionospheric response to the 2015 St. Patrick's Day storm: A global multi-instrumental overview. *J Geophys Res Space Phys* **120**: 9023–9037. https://doi.org/10.1002/2015JA021629.

Beach, TL. 2006. Perils of the GPS phase scintillation index (σ_ϕ). *Radio Sci.* **41**: RS5S31. https://doi:10.1029/2005RS003356.

Berdermann, J, Kriegel M, Banys D, Heymann F, Hoque MM, Wilken V, Borries C, Heßelbarth A, Jakowski N. 2018. Ionospheric response to the X9.3 Flare on 6 September 2017 and its implication for navigation services over Europe. *Space Weather* **16**: 1604–1615, https://doi.org/10.1029/2018SW001933.

Cameron, TG, Fiori RAD, Perry GW, Ruck JJ, Thayaparan T. 2024. High-Latitude off-great circle propagation associated with the solar terminator. *Radio Sci* **59**: e2023RS007917. https://doi.org/10.1029/2023RS007917.

Carrano, CS, Groves KM, Rino CL. 2019. On the relationship between the rate of change of total electron content index (ROTI), irregularity strength (C_kL), and the scintillation index (S4). *J Geophys Res Space Phys* **124**: 2099–2112. https://doi.org/10.1029/2018JA026353.

Cesaroni, C, Spogli L, Alfonsi L, De Franceschi G, Ciraolo L, Galera Monico JF, Scotto C, Romano V, Aquino M, Bougard B. 2015. L-band scintillations and calibrated total electron content gradients over Brazil during the last solar maximum. *J Space Weather Space Clim* **5**: A36. https://doi.org/10.1051/swsc/2015038.

De Franceschi, G, Alfonsi L, Romano V, Aquino M, Dodson A, Mitchell CN, Spencer P, Wernik AW. 2008. Dynamics of high-latitude patches and associated small-scale irregularities during the October and November 2003 storms. *J Atmos Sol-Terr Phys* **70 (6)**: 879–888. https://doi.org/10.1016/j.jastp.2007.05.018.

Fejer, BG, Navarro LA, Chakrabarty D. 2024. Recent results and outstanding questions on the response of the electrodynamics of the low latitude ionosphere to solar wind and magnetospheric disturbances. *Front Astron Space Sci* **11**: 1471140. https://doi.org/10.3389/fspas.2024.1471140.

Foelsche, U, Kirchengast G. 2002. A simple "geometric" mapping function for the hydrostatic delay at radio frequencies and assessment of its performance. *Geophys Res Lett*, **29 (10)**: 111. https://doi.org/10.1029/2001GL013744.

Friis-Christensen, E, Lühr H, Knudsen D, Haagmans R. 2008. Swarm – an Earth observation mission investigating geospace. *Adv Space Res*, **41 (1)**: 210–216.

Gonzalez-Esparza, JA, Sanchez-Garcia E, Sergeeva M, Corona-Romero P, Gonzalez-Mendez LX, et al. 2024. The Mother's Day geomagnetic storm on 10 May 2024: Aurora observations and low latitude space weather effects in Mexico. *Space Weather* **22**: e2024SW004111. https://doi.org/10.1029/2024SW004111.

Grandin, M, Bruus E, Ledvina VE, Partamies N, Barthelemy M, et al. 2024. The Gannon Storm: citizen science observations during the geomagnetic superstorm of 10 May 2024. *Geosci Commun* **7**: 297–316. https://doi.org/10.5194/gc-7-297-2024.

Groves, KM, Basu S, Weber EJ, Smitham M, Kuenzler H, et al. 1997. Equatorial scintillation and systems support. *Radio Sci* **32**: 2047–2064. https://doi.org/10.1029/97RS00836.

Hernández-Pajares, M, García-Rigo AJ, Juan JM, Sanz J, Monte E, Aragón-Ángel A. 2012. GNSS measurement of EUV photons flux rate during strong and mid solar flares. *Space Weather* **10**: S12001. https://doi.org/10.1029/2012SW000826.

Jakowski, N, Borries C, Wilken V. 2012. Introducing a disturbance ionosphere index. *Radio Sci* **47**: RS0L14. https://doi.org/10.1029/2011RS004939.

Jakowski, N, Hoque MM. 2019. Estimation of spatial gradients and temporal variations of the total electron content using ground based GNSS measurements. *Space Weather* **17**: 2. https://doi.org/10.1029/2018SW002119.

Jakowski N, Mayer C, Borries C, Pannowitsch T. 2009. Large and mid-scale ionospheric perturbation characteristics deduced from GNSS measurements. In: *The Institution of Engineering and Technology 11th International Conference on Ionospheric Radio Systems and Techniques (IRST 2009)*, pp. 1–5. https://doi.org/10.1049/cp.2009.0065.

Jakowski, N, Stankov SM, Schlueter S, Klaehn D. 2006. On developing a new ionospheric perturbation index for space weather operations. *Adv Space Res* **38 (11)**: 2596–2600. https://doi.org/10.1016/j.asr.2005.07.043.

Jayachandran, PT, Hosokawa K, Shiokawa K, Otsuka Y, Watson C, Mushini SC, MacDougall JW, Prikryl P, Chadwick R, Kelly TD. 2012. GPS total electron content variations associated with poleward moving Sun-aligned arcs. *J Geophys Res* **117**: A05310. https://doi.org/10.1029/2011JA017423.

Jin, Y, Kotova D, Xiong C, Brask SM, Clausen LBN, Kervalishvili G, Stolle C, Miloch WJ. 2022. Ionospheric plasma IRregularities – IPIR – Data product based on data from the Swarm satellites. *J Geophys Res Space Phys* **127**: e2021JA030183. https://doi.org/10.1029/2021JA030183.

Jin, Y, Xiong C, Clausen L, Spicher A, Kotova D, Brask S, Kervalishvili G, Stolle C, Miloch W. 2020. Ionospheric plasma irregularities based on in situ measurements from the Swarm satellites. *J Geophys Res Space Phys* **124**, e2020JA028103. https://doi.org/10.1029/2020JA028103.

Kataoka, R, Reddy SA, Nakano S, Pettit J, Nakamura Y. 2024. Extended magenta aurora as revealed by citizen science. *Sci Rep* **14**: 25849–25849. https://doi.org/10.1038/s41598-024-75184-9.

Kintner, PM, Ledvina BM, de Paula ER. 2007. GPS and ionospheric scintillations. *Space Weather* **5**, S09003. https://doi:10.1029/2006SW000260.

Klobuchar, JA. 1987. Ionospheric time-delay algorithm for single-frequency GPS users. *IEEE Trans Aerospace Electronic Syst – AES* **23 (3)**: 325–331. https://doi.org/10.1109/TAES.1987.310829.

Kwak, Y-S, Kim J-H, Kim S, Miyashita Y, Yang T, et al. 2024. Observational overview of the May 2024 G5-level geomagnetic storm: from solar eruptions to terrestrial consequences. *J Astron Space Sci* **41 (3)**: 171–194. https://doi.org/10.5140/JASS.2024.41.3.171.

Li, C, Hancock CM, Hamm NAS, Veettil SV, You C. 2020. Analysis of the relationship between scintillation parameters, multipath and ROTI. *Sensors* **20 (10)**: 2877. https://doi.org/10.3390/s20102877.

Liu, Y, Xie W, Xiong C, Ye T, Wang Y, Wan X, Cao Y. 2022. Distribution characteristics of the plasma irregularities inside the mid-latitude ionospheric trough based on Swarm in situ measurements. *Space Weather* **20**: e2021SW002991. https://doi.org/10.1029/2021SW002991.

Lomidze, L, Knudsen DJ, Burchill J, Kouznetsov A, Buchert S. 2018. Calibration and validation of Swarm plasma densities and electron temperatures using ground-based radars and satellite radio occultation measurements. *Radio Sci* **53**: 15–36. https://doi.org/10.1002/2017RS006415.

Lovati, G, De Michelis P, Consolini G, Berrilli F. 2022. Pressure-gradient current at high latitude from Swarm measurements. *Remote Sens* **14**: 1428. https://doi.org/10.3390/rs14061428.

Luo, X, Xiong C, Gu S, Lou Y, Stolle C, Wan X, Liu K, Song W. 2019. Geomagnetically conjugate observations of equatorial plasma irregularities from Swarm constellation and ground-based GPS stations. *J Geophys Res Space Phys* **124**: 3650–3665. https://doi.org/10.1029/2019JA026515.

Ma, G, Maruyama T. 2003. Derivation of TEC and estimation of instrumental biases from GEONET in Japan. *Ann Geophys* **21**: 2083–2093. https://doi.org/10.5194/angeo-21-2083-2003.

Maurya, AK, Venkatesham K, Kumar S, Singh R, Tiwari P, Singh AK. 2018. Effects of St. Patrick's Day geomagnetic storm of March 2015 and of June 2015 on low-equatorial D region ionosphere. *J Geophys Res Space Phys* **123**: 6836–6850. https://doi.org/10.1029/2018JA025536.

Morozova, A, Spogli L, Barata T, Imam R, Pica E, Cahuasquí JA, Hoque MM, Jakowski N, Estaço D. 2025. Scintillations in Southern Europe during the geomagnetic storm of June 2015: analysis of a plasma bubbles spill-over using ground-based data. *Remote Sens* **17**: 535. https://doi.org/10.3390/rs17030535.

Nava, B, Rodríguez-Zuluaga J, Alazo-Cuartas K, Kashcheyev A, Migoya-Orué Y, Radicella SM, Amory-Mazaudier C, Fleury R. 2016. Middle- and low-latitude ionosphere response to 2015 St. Patrick's Day geomagnetic storm. *J Geophys Res Space Phys* **121**: 3421–3438. https://doi.org/10.1002/2015JA022299.

Nayak, C, Buchert S, Yiğit E, Ankita M, Singh S, Tulasi Ram S, Dimri AP. 2025. Topside low-latitude ionospheric response to the 10–11 May 2024 super geomagnetic storm as observed by Swarm: The strongest storm-time super-fountain during the Swarm era? *J Geophys Res Space Phys* **130**: e2024JA033340. https://doi.org/10.1029/2024JA033340.

Nykiel, G, Cahuasquí JA, Hoque MM, Jakowski N. 2024. Relationship between GIX, SIDX, and ROTI ionospheric indices and GNSS precise positioning results under geomagnetic storms. *GPS Solu* **28**: 69. https://doi.org/10.1007/s10291-023-01611-5.

Olwendo, JO, Cilliers P, Weimin Z, Ming O, Yu X. 2018. Validation of ROTI for ionospheric amplitude scintillationmeasurements in a low-latitude region over Africa. *Radio Sci* **53**: 876. https://doi.org/10.1029/2017RS006391.

Orr, L, Beggan C, Brown W. 2024. A regional space weather hazard variation index utilising Swarm FAST data. *J Space Weather Space Clim* **14**: **30**. https://doi.org/10.1051/swsc/2024033.

Park, J, Lühr H, Kervalishvili G, Rauberg J, Stolle C, Kwak Y-S, Lee WK. 2017. Morphology of high-latitude plasma density perturbations as deduced from the total electron content measurements onboard the Swarm constellation. *J Geophys Res Space Phys* **122**: 1338–1359. https://doi.org/10.1002/2016JA023086.

Park, J, Noja M, Stolle C, Lühr H. 2013. The Ionospheric Bubble Index deduced from magnetic field and plasma observations onboard Swarm. *Earth Planet Space* **65**: 1333–1344. https://doi.org/10.5047/eps.2013.08.005.

Pi, X, Mannucci AJ, Lindqwister UJ, Ho CM. 1997. Monitoring of global ionospheric irregularities using the Worldwide GPS Network. *Geophys Res Lett* **24**: 2283–2286. https://doi.org/10.1029/97GL02273.

Prol, FS, Pignalberi A, Smirnov A, Pezzopane M, Christovam AL, Selvan K, Hoque M, Kaasalainen S. 2025. Ionospheric tomography for Swarm satellite orbit determination using single-frequency GNSS data. *GPS Solu* **29**: 26. https://doi.org/10.1007/s10291-024-01779-4.

Sharma, AK, Gurav OB, Gaikwad HP, Chavan GA, Nade DP, Nikte SS, Ghodpage RN, Patil PT. 2018. Study of equatorial plasma bubbles using all sky imager and scintillation technique from Kolhapur station: a case study. *Astrophys Space Sci* **363**: 83. https://doi.org/10.1007/s10509-018-3303-4.

Spogli, L, Alberti T, Bagiacchi P, Cafarella L, Cesaroni C, et al. 2024. The effects of the May 2024 Mother's Day superstorm over the Mediterranean sector: from data to public communication. *Ann Geophys* **67 (2)**: 218. https://doi.org/10.4401/ag-9117.

Thaganyana, GP, Habarulema JB, Ngwira C, Azeem I. 2022. Equatorward medium to large-scale traveling ionospheric disturbances of high latitude origin during quiet conditions. *J Geophys Res Space Phys* **127**: e2021JA029558. https://doi.org/10.1029/2021JA029558.

Van Dierendonck AJ, Klobuchar J, Hua Q. 1993. Ionospheric scintillation monitoring using commercial single frequency C/A Code Receivers. In: *Proceedings of the 6th International Technical Meeting of the Satellite Division of The Institute of Navigation (ION GPS 1993)*, pp. 1333–1342.

Vasylyev, D, Cahuasquí JA, Hoque M, Jakowski N, Kriegel M, David P, Tagargouste Y, Buchert S, Berdermann J. 2024. Scintillation modeling with random phase gradient screens. *J Space Weather Space Clim* **14**: 29. https://doi.org/10.1051/swsc/2024028.

Wilken, V, Kriegel M, Jakowski N, Berdermann J. 2018. An ionospheric index suitable for estimating the degree of ionospheric perturbations. *J Space Weather Space Clim* **8**: A19. https://doi.org/10.1051/swsc/2018008.

Wu, DL. 2020. Ionospheric S4 Scintillations from GNSS Radio Occultation (RO) at Slant Path. *Remote Sens* **12**: 15. https://doi.org/10.3390/rs12152373.

Xiong, C, Stolle C, Lühr H, Park J, Fejer BG, Kervalishvili GN. 2016a. Scale analysis of equatorial plasma irregularities derived from Swarm constellation. *Earth Planet Space* **68**: 121. https://doi.org/10.1186/s40623-016-0502-5.

Xiong, C, Xu J, Wu K, Yuan W. 2018. Longitudinal thin structure of equatorial plasma depletions coincidently observed by Swarm constellation and all-sky imager. *J Geophys Res Space Phys* **123**: 1593–1602. https://doi.org/10.1002/2017JA025091.

Xiong, C, Zhou Y-L, Lühr H, Ma S-Y. 2016b. Diurnal evolution of the F region electron density local time gradient at low and middle latitudes resolved by the Swarm constellation. *J Geophys Res Space Phys* **121**: 9075–9089. https://doi.org/10.1002/2016JA023034.

Zhao, D, Li W, Li C, Tang X, Wang Q, Hancock CM. 2022. Ionospheric phase scintillation index estimation based on 1 Hz geodetic GNSS receiver measurements by using continuous wavelet transform. *Space Weather* **20**: e2021SW003015. https://doi.org/10.1029/2021SW003015.

Zhou, Y-L, Lühr H, Alken P, Xiong C. 2016. New perspectives on equatorial electrojet tidal characteristics derived from the Swarm constellation. *J Geophys Res Space Phys* **121**: 7226–7237. https://doi.org/10.1002/2016JA022713.

Cite this article as: Cahuasquí JA, Hoque MM, Jakowski N, Buchert S, Vasylyev D, et al. 2025. New Swarm products NeGIX and TEGIX for monitoring horizontal ionospheric gradients. *J. Space Weather Space Clim.* **15**, 45. https://doi.org/10.1051/swsc/2025040.

Appendix A: Description of variables in the daily NeGIX data product

Name	Description	Unit
Timestamp	Time in Universal Time	
Longitude	Position of NeGIX in geocentric longitude. Averaged longitude position of the central points (CPs) derived from the combination of Ne measurements of Swarm A and C.	deg
Latitude	Position of NeGIX in geocentric latitude. Averaged latitude position of the central points (CPs) derived from the combination of Ne measurements of Swarm A and C.	deg
Distance	Averaged distance (Δs) value from all dipoles used for the estimation of NeGIX values	m
Azimuth	Averaged azimuth (δ) value from all dipoles used for the estimation of NeGIX values	deg
Negix_X	Mean value of NeGIX for the West-East component	$cm^{-3}\ m^{-1}$
Negix_X_Sigma	Standard deviation value of NeGIX for the West-East component	$cm^{-3}\ m^{-1}$
Negix_X_P95	95th-percentile value of NeGIX for the West-East component	$cm^{-3}\ m^{-1}$
Negix_Y	Mean value of NeGIX for the South-North component	$cm^{-3}\ m^{-1}$
Negix_Y_Sigma	Standard deviation value of NeGIX for the South-North component	$cm^{-3}\ m^{-1}$
Negix_Y_P95	95th-percentile value of NeGIX for the South-North component	$cm^{-3}\ m^{-1}$
Negix_Total	Total vector value of NeGIX, derived from the mean West-East and South-North components	$cm^{-3}\ m^{-1}$
Negix_Sigma	Vector value of the standard deviation of NeGIX, derived from the standard deviation values of West-East and South-North components	$cm^{-3}\ m^{-1}$
Negix_P95	Vector value of the 95th-percentile of NeGIX, derived from the 95th-percentile values of West-East and South-North components	$cm^{-3}\ m^{-1}$
N_Measurements	Number of elements for a data record from which NeGIX is determined	
Flag_Negix	Flags characterizing the dispersion of gradient values that are used to compute the total vector Negix_Total	
Orbit_Label	Value defining whether the magnitude belongs to an ascending or descending orbit of the Swarm satellites	

Appendix B: Description of variables in the daily TEGIX data product

Further information about the definition of the MIGRAS products can be found on ESA's webpage at https://earth.esa.int/eogateway/ activities/ migras.

Name	Description	Unit
Timestamp	Time in Universal Time	
Longitude_Swarm	Averaged geocentric longitude of the Swarm satellites for all combined measurements for a certain epoch	deg
Latitude_Swarm	Averaged geocentric latitude of the Swarm satellites for all combined measurements for a certain epoch	deg
Longitude_IPPs	Position of TEGIX in geocentric longitude. Averaged longitude position of the central points (CPs) derived from the combination of VTEC measurements of Swarm A and C.	deg
Latitude_IPPs	Position of TEGIX in geocentric latitude. Averaged latitude position of the central points (CPs) derived from the combination of VTEC measurements of Swarm A and C.	deg
Distance	Averaged distance (Δs) value from all dipoles used for the estimation of TEGIX values	m
Azimuth	Averaged azimuth (δ) value from all dipoles used for the estimation of TEGIX values	deg
Tegix_X	Mean value of TEGIX for the West-East component	milli-TECU m^{-1}
Tegix_X_Sigma	Standard deviation value of TEGIX for the West-East component	milli-TECU m^{-1}
Tegix_X_P95	95th-percentile value of TEGIX for the West-East component	milli-TECU m^{-1}
Tegix_Y	Mean value of TEGIX for the South-North component	milli-TECU m^{-1}
Tegix_Y_Sigma	Standard deviation value of TEGIX for the South-North component	milli-TECU m^{-1}
Tegix_Y_P95	95th-percentile value of TEGIX for the South-North component	milli-TECU m^{-1}
Tegix_Total	Total vector value of TEGIX, derived from the mean West-East and South-North components	milli-TECU m^{-1}
Tegix_Sigma	Vector value of the standard deviation of TEGIX, derived from the standard deviation values of West-East and South-North components	milli-TECU m^{-1}
Tegix_P95	Vector value of the 95th-percentile of TEGIX, derived from the 95th-percentile values of West-East and South-North components	milli-TECU m^{-1}
N_Measurements	Number of elements for a data record from which TEGIX is determined	
Flag_Tegix	Flags characterizing the dispersion of gradient values that are used to compute the total vector Tegix_Total	
Orbit_Label	Value defining whether the magnitude belongs to an ascending or descending orbit of the Swarm satellites	